J. Fluid Mech. (2009), *vol.* 633, *pp.* 115–135.
doi:10.1017/S0022112009007460 Printed in the United Kingdom

A two-phase flow description of the initiation of underwater granular avalanches

MICKAËL PAILHA† AND OLIVIER POULIQUEN

Laboratoire IUSTI, UMR 6595 CNRS, Aix Marseille Université (UI, UII),
5 rue Enrico Fermi, 13465 Marseille cedex 13, France

(Received 10 October 2008 and in revised form 12 March 2009)

A theoretical model based on a depth-averaged version of two-phase flow equations is developed to describe the initiation of underwater granular avalanches. The rheology of the granular phase is based on a shear-rate-dependent critical state theory, which combines a critical state theory proposed by Roux & Radjai (1998), and a rheological model recently proposed for immersed granular flows. Using those phenomenological constitutive equations, the model is able to describe both the dilatancy effects experienced by the granular skeleton during the initial deformations and the rheology of wet granular media when the flow is fully developed. Numerical solutions of the two-phase flow model are computed in the case of a uniform layer of granular material fully immersed in a liquid and suddenly inclined from horizontal. The predictions are quantitatively compared with experiments by Pailha, Nicolas & Pouliquen (2008), who have studied the role of the initial volume fraction on the dynamics of underwater granular avalanches. Once the rheology is calibrated using steady-state regimes, the model correctly predicts the complex transient dynamics observed in the experiments and the crucial role of the initial volume fraction. Quantitative predictions are obtained for the triggering time of the avalanche, for the acceleration of the layer and for the pore pressure.

1. Introduction

Debris flows (Iverson 1997), landslides (Legros 2002) or submarine avalanches (Hampton, Lee & Locat 1996) are catastrophic events characterized by the flow of a mixture of liquid and particles down a slope. Understanding how these complex media propagate remains a real challenge. The first approach consists in modelling the mixture as a non-Newtonian fluid described by a Bingham or a Hershel Bulkley rheology (Imran *et al.* 2001; Pastor *et al.* 2004). Although relevant for pure mud flows, the single phase approach is found inappropriate when granular materials are involved (Iverson 1997; Iistad *et al.* 2004). In this case, a relative motion between the fluid phase and the granular skeleton often develops, which induces gradients of fluid pressure and dramatically affect the flow (Rice 1975; Rudnicki 1984; Iverson & Lahusen 1989).

The relative motion between the fluid and the granular matrix can be created by different mechanics: the development of gradients of hydrostatic pressure when the surface of the liquid is inclined from horizontal (Iverson 2000; Okura *et al.* 2002), the presence of underground springs and the presence of heterogeneities in the granular

† Email address for correspondence: mickael.pailha@etu.univ-provence.fr

media (Major & Iverson 1999). Another mechanism important for the initiation of flow, is the change of solid volume fraction experienced by the granular skeleton when it starts flowing. Granular materials are known to change volume when sheared (Reynolds 1886; Schofield & Wroth 1968; Wood 1990): a dense packing dilates and a loose packing compacts. When the material is saturated with a fluid, the change in volume fraction induces a fluid motion and a pore pressure gradient, which can in turn affect the deformation (Iverson *et al.* 2000; Iverson 2005). In case of a dilatation, the liquid is sucked into the medium, pressing the grains together and enhancing the friction, whereas in case of a compaction, the liquid is expelled decreasing the frictional interactions. This coupling between the dilatancy and the pore pressure is called 'pore pressure feedback' (Iverson 2005; Schaeffer & Iverson 2008) and has a dramatic influence in the way a landslide starts, as evidenced by the experiment carried out by Iverson *et al.* in the USGS large-scale facility (Iverson *et al.* 2000). The authors have shown that samples of soil prepared on a slope with different initial volume fractions behave differently when submitted to a rainfall. Initially loose soils suddenly liquefy and rapidly flow, whereas dense samples merely creep slowly.

Recently, we have been able to put in evidence the crucial role of the initial volume fraction on underwater avalanches in a small-scale laboratory experiment (Pailha, Nicolas & Pouliquen 2008). The experiment consists of a box full of liquid and grains. The sediment layer is prepared at a controlled initial volume fraction and is suddenly inclined from horizontal. The pore pressure and the motion of the granular layer are simultaneously monitored from the beginning of the inclination to the development of a steady flow regime. We have shown that a slight change in the initial volume fraction significantly affects the avalanche dynamics, and that a delay in the triggering of the avalanche can be induced by initially compacting the sediment. The variation of the avalanching time with the control parameters (Pailha *et al.* 2008) can be understood based on simple arguments involving the dilatancy of the granular layer and the coupling with the interstitial fluid. However, in order to capture the whole dynamics from the initiation to the steady flow, a complete theory has yet to be developed. This is the main purpose of this paper. A two-phase flow model is proposed, which is quantitatively compared with the avalanche dynamics measured in the experiments of Pailha *et al.* (2008).

Several theoretical studies have been developed to describe debris flows, based on two-phase flow equations (Jackson 1997, 2000). Berzi & Jenkins (2008*a*, *b*) have considered the problem of steady and fully developed flows of particles and fluid down a slope. They made the assumption that the fluid phase rheology is described by an eddy viscosity and the granular phase by a shear-rate-dependent friction law (Da Cruz *et al.* 2005; Jop, Forterre & Pouliquen 2006). This approach successfully describes the velocity and density profiles observed in the experiments by Armanini *et al.* (2005), in which a mixture of grains and water is continuously injected at the top of a slope. This approach is for the moment restricted to steady and fully developed flows and does not take into account dilatancy effects.

Iverson & Denliger (2001*a*, *b*) and Pitman & Le (2005) have developed a depth-averaged version of the two-phase flow equations, assuming that the flowing layer is thin. This model is tractable to describe unsteady and non-uniform configurations encountered in real geophysical flows. In their work, the granular phase is described as a Coulomb material, and again, no dilatancy is present.

The dilatancy of the granular layer and the pore pressure feedback mechanism are taken into account in the models developed by Iverson (Iverson 2005; Schaeffer &

Iverson 2008). In this approach, the landslide is described as a rigid block sliding down a slope, the source of dilatancy being localized at the base. The pore pressure builds up at the base and is assumed to diffuse through the block, following a classical consolidation equation based on the assumption that the block behaves as a poro-elastic medium. A limit of this approach is that the long time evolution and the fully developed regime cannot be described, no shear rate dependence being incorporated in the rheology.

In order to model our underwater avalanche experiments, it is necessary to combine elements from the different theories. First, we are going to use the framework of the depth-averaged equations developed by Pitman & Le (2005). Although the theory does not provide a detailed description of the flow inside the layer, it represents a first approach, in which new constitutive equations for the granular phase can be easily implemented. Secondly, we need to describe the dilatation or compaction linked to the initial deformation of the granular layer as in Iverson's model (Iverson 2005). Critical state theories developed in soil mechanics are effective ways to describe the change in volume fraction (Schofield & Wroth 1968; Wood 1990; Roux & Radjai 1998). However, such theories are independent of shear rate and need to be adapted to rapid deformations. The last ingredient we need is a relevant rheology for the granular phase in order to capture the fully developed flows as in the work by Berzi & Jenkins (2008). The rheology of a mixture of grains and fluid is still an open problem. It has been extensively studied but mostly in a dilute regime, when particles interact through hydrodynamics interactions (Brady & Bossis 1988; Morris & Boulay 1999). However, at higher concentrations as the one encountered in our system, contacts between the grains exist, and the frictional interactions become predominant (Ancey, Coussot & Evesque 1999; Huang *et al.* 2005). In this regime, recent experiments have been conducted in different configurations like inclined planes (Cassar, Nicolas & Pouliquen 2005), rotating drums (Courech du Pont *et al.* 2003; Jain, Ottino & Lueptow 2004), plane shear (Géminard, Losert & Gollub 1999) and surface flows on a pile (Doppler *et al.* 2007). It has been shown that a shear-rate-dependent friction law similar to the one obtained in dry granular flows could be relevant (Cassar *et al.* 2005; Doppler *et al.* 2007). In the model presented in this paper, we adopt this shear-rate-dependent friction law to describe the steady-state rheology of our granular underwater avalanches.

Our approach consists in coupling the wet granular rheology with the critical state theory in order to obtain new constitutive laws for the granular phase, which describe both the initial dilatancy and the steady state. These constitutive laws are introduced in two-phase flow equations to capture the pore pressure feedback mechanism and model the triggering of underwater avalanches.

The paper is organized as follows: In § 2 we present the main observations obtained in our previous experimental work concerning the role of the initial volume fraction on the initiation of submarine avalanches. In § 3, the two-phase flow model and the constitutive laws of the granular phase are derived. In § 4, a quantitative comparison with the experimental measurements is presented, where special care is taken in the calibration of the parameters introduced in the model. Discussion and conclusions are given in § 5.

2. Summary of the experimental observations

The details of the experimental set-up are given in Pailha *et al.* (2008). It consists of a long box filled with liquid and grains, which can freely rotate around the y-axis

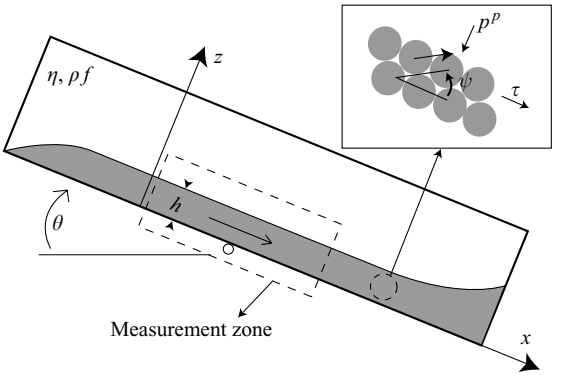

FIGURE 1. Sketch of the experimental configuration.

(figure 1). The grains used are glass beads of density $\rho_s = 2500\,\mathrm{g\,m^{-3}}$ and $d = 160$ μm in mean diameter. The liquid is a mixture of Water and Ucon oil 75H90000, a viscous water-soluble fluid. Two mixtures have been used: a low viscosity mixture ($\eta = 9.8 \times 10^{-3}$Pa s) and a high viscosity mixture ($\eta = 96 \times 10^{-3}$Pa s). The set-up is initially in a horizontal position with a uniform layer of sediment prepared in a loose state after sedimentation. The initial volume fraction ϕ_0 is then precisely adjusted by imposing taps of controlled amplitude on the box. Once the desired initial state is obtained, the set-up is tilted at a given inclination θ from horizontal. In the central zone where the flow remains uniform, we then record the basal fluid pressure $p_b^f(t)$ below the layer and the velocity $u_s^p(t)$ of the particles at the free surface. For a given set of fluid and grains, the control parameters are the amount of grains in the box measured by the initial thickness h_0, the initial volume fraction ϕ_0 and the inclination angle θ.

Typical results obtained for different initial volume fractions are presented in figures 2(a, b) and 3(a, b) for the two viscosities used. The main observations are the following. The behaviour can be roughly divided in a dense and a loose behaviour corresponding to ϕ_0 greater or less than 0.58. The dense behaviour (continuous lines in figures 2 and 3) is characterized by an initial slow creep, which can last more than 3 min (figure 3a), followed by an increase of the velocity, which ultimately seems to reach a plateau corresponding to a steady regime. The pore pressure in this case is initially negative, a signature of the liquid being sucked into the granular layer when it is dilating. The loose case (dotted lines in figures 2 and 3) corresponds to an initial rapid acceleration followed by a relaxation to the steady state. In the loosest cases, the transient velocity can be higher than the steady-state value. When an overshoot in velocity is observed, the measured pore pressure is positive corresponding to an expulsion of the fluid during the compaction (figure 3b).

In Pailha *et al.* (2008), we have systematically analysed how the time delay before the avalanche starts varies with the experimental parameters and how the pore pressure varies. An argument based on the granular dilatancy and on a Darcy law describing the fluid flow through the grains explains the observed scaling. In this study, we develop a complete two-phase flow model able to describe the whole dynamics in both the dense and loose cases, from the initiation to the steady-state regime.

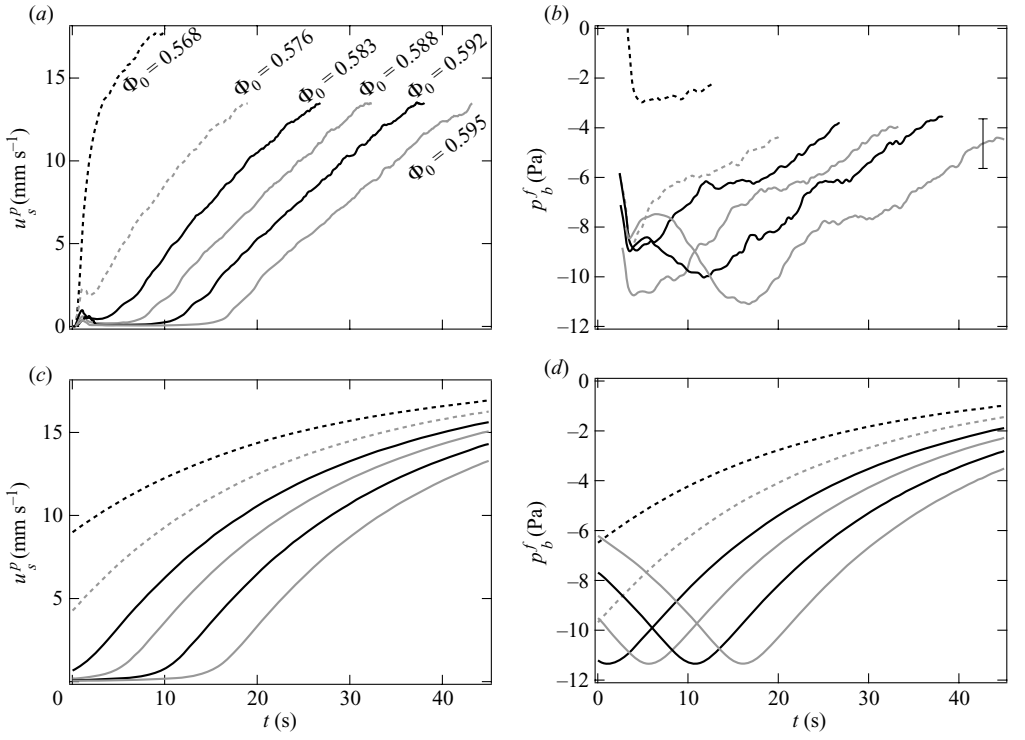

FIGURE 2. Time evolution of the particle free surface velocity u_s^p and of the basal pore pressure p_b^f for different initial volume fraction for the low viscosity fluid, $h = 6.1$ mm, $\theta = 28°$; (a, b) experiments; (c, d) predictions of the model; dotted lines mean loose behaviours, solid lines mean dense behaviours. The error bar corresponds to the sensitivity of the pressure sensor.

3. Theoretical description

In order to capture the rich dynamics observed in our system, the theoretical model should contain several ingredients. First, it has to be written in terms of two-phase flow equations to capture the coupling between the fluid and the granular skeleton. Secondly, the model should be able to predict the correct steady state. This means that the rheology of the granular phase has to be correctly taken into account. Thirdly, the compaction or dilatation, which takes place at the beginning of the deformation has to be described. In this section we show step by step how to build a minimum model, which takes into account all these ingredients.

3.1. *Depth-averaged two-phase flow equations*

In two-phase flow equations the grains and the fluid are described as two continuum phases characterized by different velocities, by different stresses and interacting through hydrodynamic forces. The mass and momentum conservation laws can be formally derived from local averaging (Jackson 2000), the problem being the choice of the constitutive laws for each phase and the choice of the interacting forces. In order to model the configuration of a thin immersed granular layer flowing on an inclined plane, we follow the work by Pitman & Le (2005), who derive a depth-averaged version of the two-phase flow equations of Jackson (2000).

Let us consider a granular layer of thickness h fully immersed in a fluid of density ρ_f and viscosity η on a plane inclined at an angle θ from horizontal (figure 1).

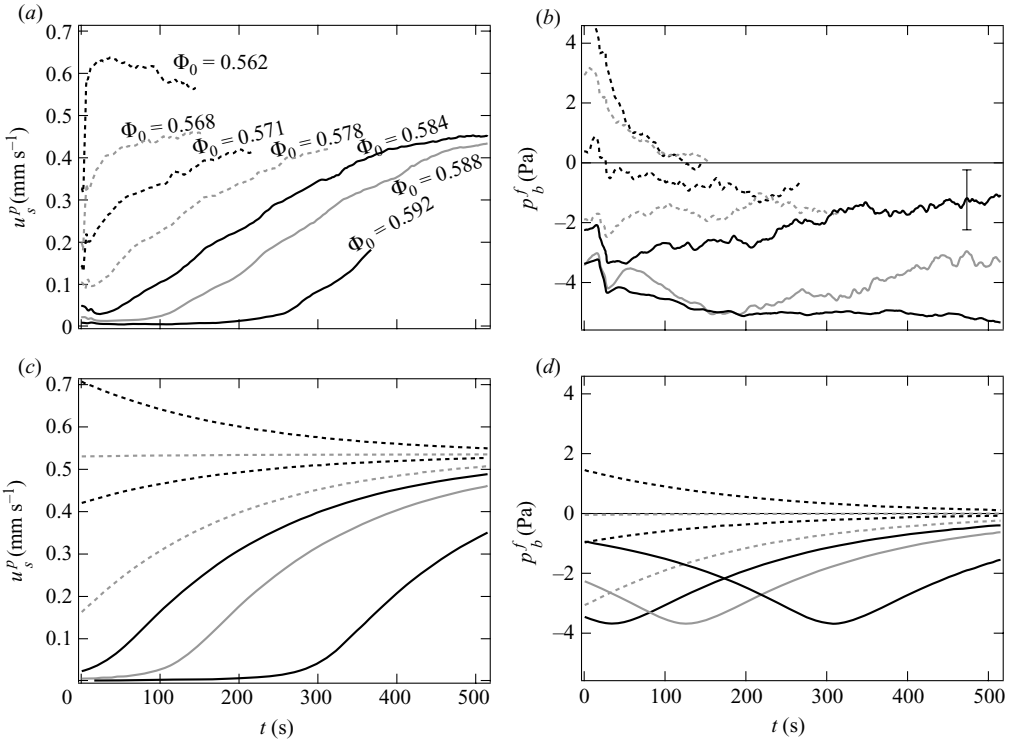

FIGURE 3. Time evolution of the particle free surface velocity u_s^p and of the basal pore pressure p_b^f for different initial volume fraction for the high viscosity fluid, $h = 4.9$ mm, $\theta = 25°$; (a, b) experiments; (c, d) predictions of the model; dotted lines mean loose behaviours, solid lines mean dense behaviours. The error bar corresponds to the sensitivity of the pressure sensor.

Particle diameter is d and ρ_p is the density of the particles. We assume the flow to be uniform in the x-direction. However, motion in the z-direction exists, which is induced by the dilatation or the compaction of the granular layer. The volume fraction of the granular packing is $\phi(z, t)$. The particle and fluid velocities are, respectively, $\boldsymbol{u}^p = u^p(z, t)\boldsymbol{e}_x + v^p(z, t)\boldsymbol{e}_z$ and $\boldsymbol{u}^f = u^f(z, t)\boldsymbol{e}_x + v^f(z, t)\boldsymbol{e}_z$ with $\boldsymbol{e}_x$ and $\boldsymbol{e}_z$ being the unit vectors along the x- and z-axes. The tensors $\boldsymbol{\sigma}^p$ and $\boldsymbol{\sigma}^f$ are the particle and fluid stress tensors, respectively.

The mass and momentum conservation equations for the two phases are given by the following expressions:

$$\frac{\partial \phi}{\partial t} + \nabla \cdot (\boldsymbol{u}^p \phi) = 0, \tag{3.1}$$

$$\frac{\partial (1-\phi)}{\partial t} + \nabla \cdot (\boldsymbol{u}^f (1-\phi)) = 0, \tag{3.2}$$

$$\rho_p \phi \left(\frac{\partial \boldsymbol{u}^p}{\partial t} + \boldsymbol{u}^p \cdot \nabla \boldsymbol{u}^p \right) = \nabla \cdot \boldsymbol{\sigma}^p + \phi \nabla \cdot \boldsymbol{\sigma}^f + \boldsymbol{f} + \rho_p \phi \boldsymbol{g}, \tag{3.3}$$

$$\rho_f (1-\phi) \left(\frac{\partial \boldsymbol{u}^f}{\partial t} + \boldsymbol{u}^f \cdot \nabla \boldsymbol{u}^f \right) = (1-\phi) \nabla \cdot \boldsymbol{\sigma}^f - \boldsymbol{f} + \rho_f (1-\phi) \boldsymbol{g}. \tag{3.4}$$

The term $\boldsymbol{f}$ includes the interaction forces between the two phases, beside the buoyancy $\phi\nabla\cdot\boldsymbol{\sigma}^f$. Notice that we have written the buoyancy using the whole stress tensor and not only the isotropic part, a choice explained by Jackson in his book (Jackson 2000). For the viscous drag $\boldsymbol{f}$, we adopt the simple formulation given by

$$\boldsymbol{f} = (1-\phi)^2\beta(\boldsymbol{u}^f - \boldsymbol{u}^p)$$

with $\beta = \eta/(\alpha d^2)$, where αd^2 is the permeability of the porous media formed by the particles (Ouriemi, Aussillous, & Guazzelli in press). Here for α we use the Kozeny–Carman formula for packing of spheres: $\alpha = (1-\phi)^3/150\phi^2$.

The underwater avalanches belong to a dense granular flow regime, in which the stress related to the contact interactions between the particles is predominant compared to all other viscous stresses, which develop in the fluid phase (see appendix C). Following several authors (Iverson 2005; Pitman & Le 2005), we then assume that the viscous stresses in the fluid phase are negligible. Under this assumption, the fluid stress tensor simply reduces to the isotropic pressure part, which can then be written as $\boldsymbol{\sigma}^f = -(p^f + p^{hydro})\boldsymbol{I}$, where p^{hydro} is the hydrostatic part, which verifies $\nabla\cdot p^{hydro} = \rho_f \boldsymbol{g}$. Under this assumption and using the uniformity of the flow in the x-direction, the momentum equations then reduce to the following equations:

$$\rho_p\phi\left(\frac{\partial u^p}{\partial t} + v^p\frac{\partial u^p}{\partial z}\right) = \frac{\partial \sigma^p_{xz}}{\partial z} + (\rho_p-\rho_f)\phi g\sin\theta + (1-\phi)^2\beta(u^f-u^p), \quad (3.5)$$

$$\rho_p\phi\left(\frac{\partial v^p}{\partial t} + v^p\frac{\partial v^p}{\partial z}\right) = \frac{\partial \sigma^p_{zz}}{\partial z} - (\rho_p-\rho_f)\phi g\cos\theta - \phi\frac{\partial p^f}{\partial z} + (1-\phi)^2\beta(v^f-v^p), \quad (3.6)$$

$$\rho_f(1-\phi)\left(\frac{\partial u^f}{\partial t} + v^f\frac{\partial u^f}{\partial z}\right) = -(1-\phi)^2\beta(u^f-u^p), \quad (3.7)$$

$$\rho_f(1-\phi)\left(\frac{\partial v^f}{\partial t} + v^f\frac{\partial v^f}{\partial z}\right) = -(1-\phi)\frac{\partial p^f}{\partial z} - (1-\phi)^2\beta(v^f-v^p). \quad (3.8)$$

Following the work by Pitman & Le (2005), we can integrate in the depth the mass conservation (3.1) and the x momentum equations (3.5) and (3.7). Introducing the depth-averaged quantities denoted by a bar, $\overline{A}(t) = (1/h)\int_0^h A(z,t)\,\mathrm{d}z$, the equations reduce to

$$\frac{\mathrm{d}\overline{\phi}h}{\mathrm{d}t} = 0, \quad (3.9)$$

$$\rho_p\frac{\mathrm{d}\overline{\phi}h\overline{u}^p}{\mathrm{d}t} = (\rho_p-\rho_f)g\overline{\phi}h\sin\theta - \tau_b^p + \frac{150\eta\overline{\phi}^2}{(1-\overline{\phi})d^2}(\overline{u}^f-\overline{u}^p)h, \quad (3.10)$$

$$\rho_f\frac{\mathrm{d}(1-\overline{\phi})h\overline{u}^f}{\mathrm{d}t} = -\frac{150\eta\overline{\phi}^2}{(1-\overline{\phi})d^2}(\overline{u}^f-\overline{u}^p)h. \quad (3.11)$$

Equation (3.10) stipulates that the solid phase acceleration is balanced by three forces: the relative gravity force, the basal frictional shear stress $\tau_b^p = \sigma^p_{xz_{|z=0}}$, which exists at the interface between the granular layer and the rough bottom and the drag force. The fluid acceleration (3.11) is simply balanced by the drag force between the two phases. Notice that writing the drag force in terms of the averaged quantities is not rigorously derived from the depth-averaging process (see Pitman & Le 2005) but is a reasonable assumption.

In writing depth-averaged momentum equations, we have hidden the complex rheological behaviour in the basal shear stress τ_b^p, which needs now to be specified. However, before going into the details of the rheology, we anticipate that the granular stress is of frictional nature, meaning that τ_b^p is linked to the particle normal stress at the base $\sigma^p_{zz_{|z=0}}$. Information about this stress component is obtained from the z momentum equations (3.6) and (3.8). In classical shallow water approximation, the vertical velocity is usually linked to the non-uniformity of the flow assumed to be small, which implies from (3.8) that the fluid pressure is simply hydrostatic ($p^f = 0$). However, in our underwater avalanches, the vertical displacement is induced by the dilatation or the compaction of the granular layer. This vertical motion is a key feature, which controls the dynamics by influencing the pressure. This coupling between the vertical displacement and the pressure comes from the last term in (3.8) and has to be considered as predominant. Under this assumption, a gradient of fluid pressure exists given by

$$\frac{\partial p^f}{\partial z} = -(1-\phi)\beta(v^f - v^p). \tag{3.12}$$

Using the fact that mass conservation implies $\phi v^p + (1-\phi)v^f = 0$, substituting expression (3.12) in (3.6) and integrating over the depth leads to the following expression for the basal particle normal stress called in the following p_b^p:

$$p_b^p = \sigma^p_{zz_{|z=0}} = (\rho_p - \rho_f)\overline{\phi} g h \cos\theta + \beta h \overline{v}^p. \tag{3.13}$$

Equations (3.9)–(3.11) and (3.13) define our depth-averaged two-phase flow model. The next step consists in expressing the granular rheology embedded in the basal stress τ_b^p and in describing how dilatation or contraction occurs.

3.2. *Granular rheology*

In the case of a dry granular material with no interstitial fluid, it has been shown (GDR MiDi 2004; Da Cruz *et al.* 2005; Forterre & Pouliquen 2008) that a granular layer continuously sheared at a shear rate $\dot{\gamma}$ under a confining pressure p^p reaches a steady state characterized by an equilibrium shear stress τ^p_{eq} and an equilibrium critical volume fraction ϕ_{eq} given by

$$\tau^p_{eq} = \mu(I) p^p \tag{3.14}$$

$$\phi_{eq} = \phi_{eq}(I) \tag{3.15}$$

where

$$I = \frac{t_{micro}}{t_{macro}} = \frac{\dot{\gamma} d}{\sqrt{p^p/\rho_p}}$$

is a dimensionless number given by the ratio of two time scales: the time scale of rearrangement $t_{micro} = d/(\sqrt{p^p/\rho_p})$ and the macroscopic time scale $t_{macro} = 1/\dot{\gamma}$. The function $\mu(I)$ is a shear-rate-dependent coefficient of friction. It tends to a constant μ_s in the quasi-static limit when I goes to zero and increases with I. The volume fraction $\phi_{eq}(I)$ is a decreasing function of I. Although this description fails in capturing all the details of granular flows close to the flow threshold, it gives quantitative predictions in several flow configurations (Forterre & Pouliquen 2008).

The case of immersed granular flows has been much less studied and the rheology is still the matter of debate. However, by analogy to the dry case, it has been proposed that a granular material sheared in the presence of an interstitial viscous liquid is also described by the same constitutive laws (3.14) and (3.15), the time scale of rearrangement t_{micro} being changed to a viscous time scale proportional to η/p^p

(Courech du Pont *et al.* 2003; Cassar *et al.* 2005) where η is the viscosity of the fluid. This approach has been used with relative success to describe steady underwater granular flows down the inclined planes (Cassar *et al.* 2005) and underwater free surface flows on a pile (Doppler *et al.* 2007). Under this assumption and for low values of I for which the functions $\mu(I)$ and $\phi_{eq}(I)$ are approximated by linear functions, the rheology of a granular material sheared in a viscous fluid under a confining pressure p^p is given by the following shear stress and volume fraction:

$$\tau_{eq}^p = \mu_s p^p + K_1 \eta \dot{\gamma}, \tag{3.16}$$

$$\phi_{eq} = \phi_c - K_2 \frac{\eta \dot{\gamma}}{p^p}, \tag{3.17}$$

where K_1 and K_2 are constant. The shear stress is then the sum of a pure frictional term and a pure viscous term. A similar Coulomb-viscous writing for the shear stress has been proposed in previous models of debris flows (Iverson 1985). In the expression for the volume fraction, we have introduced the critical value ϕ_c, which represents the critical volume fraction observed when a continuous quasi-static deformation occurs. However, depending on the preparation, a packing can be initially denser or looser than ϕ_c and will then experience dilatation or contraction before reaching the critical value ϕ_c at large deformation. The last step in the development of our model consists in modifying (3.16) and (3.17), which are valid in the steady regime only, in order to describe the initial deformation and to capture the initial changes in volume fraction.

3.3. *Dilatancy model*

A relevant framework to capture the transient deformation is the simple critical state theory proposed by Roux & Radjai (1998) and Roux & Radjai (2001) and valid for rigid particles at a low level of confining stress. The model is based on the concept of a dilatancy angle ψ, which gives the rate of dilatation (compaction) of the material under a simple shear. To understand the idea, it is useful to consider two layers of beads confined under a pressure p^p and sheared as sketched in inset of figure 1. The angle of dilatancy is the angle made by the tangential plane between the top and the bottom particles. If (X, Z) is the position of the top particle relative to the bottom one, it is easy to show that the rigidity of the particles implies that a horizontal displacement ΔX implies a vertical displacement $\Delta Z = \tan\psi \Delta X$. Moreover, if $\tan\delta$ is the friction coefficient between the particle, it is easy to show that the shear stress τ necessary to move the top layer is equal to $\tau = \tan(\delta + \psi)p^p$. This simple picture clearly shows an important property of the geometrical entanglement: the dilatation of a dense packing ($\psi > 0$) is accompanied by an increase of the apparent friction coefficient, the increase being equal to the dilatancy, whereas the compaction of a loose packing ($\psi < 0$) corresponds to a decrease of the apparent friction. Based on this picture, Roux & Radjai (1998) have written the following equation to describe the evolution of the volume fraction and of the shear stress in a granular material sheared at a shear rate $\dot{\gamma}$ under a confining pressure p^p:

$$\frac{1}{\phi}\frac{\mathrm{d}\phi}{\mathrm{d}t} = \frac{\partial v^p}{\partial z} = \tan\psi \dot{\gamma}, \tag{3.18}$$

$$\tau^p = \tan\psi p^p + \tau_{eq}^p, \tag{3.19}$$

$$\tan\psi = K_3(\phi - \phi_{eq}), \tag{3.20}$$

where τ_{eq} and ϕ_{eq} are the stress and the volume fraction obtained in the steady regime. The first equation is a rewriting of the kinematic condition $\Delta Z = \tan\psi \Delta X$

and stipulates how the dilatation or the contraction occurs depending on the value of the dilatancy angle. The second equation means that the change in volume fraction implies an additional stress contribution due to the geometrical entanglement. The last equation simply assumes that the dilatancy angle is proportional to the difference between the actual volume fraction and the critical volume fraction corresponding to the steady state, with K_3 being a constant. The linear variation of the dilatancy angle with the volume fraction can be seen as the first term of a Taylor expansion of a more general dilatancy expression $\psi(\phi)$ with $\psi(\phi_{eq})=0$ (see Roux & Radjai 1998). Under a constant imposed shear rate $\dot{\gamma}$, this set of equations predicts that the volume fraction and the shear stress relax towards the steady-state regime given by ϕ_{eq} and τ^p_{eq} with a time of relaxation simply given by $1/(K_3\phi_{eq}\dot{\gamma})$. In their original work, Roux and Radjai were interested in quasi-static flow of dry granular media and the critical shear stress and the critical volume fraction were constant. To generalize this approach to our immersed granular flows, we now assume that τ^p_{eq} and ϕ_{eq} are shear rate dependent, given by the phenomenological constitutive laws (3.16) and (3.17). Equations (3.18)–(3.20) together with (3.16) and (3.17) represent the simplest shear-rate-dependent critical state theory for granular material.

3.4. *Final model*

We now have all the ingredients to write the basal shear stress τ^p_b in the momentum equation (3.10). According to (3.16) and (3.19), τ^p_b is related to the dilatancy at the base $\tan\psi_b$, to the pressure at the base p^p_b and to the shear rate at the base $\dot{\gamma}_b$

$$\tau^p_b = (\mu_s + \tan\psi_b)p^p_b + K_1\eta\dot{\gamma}_b. \tag{3.21}$$

To close the system, we have to relate the basal quantities to the depth-averaged quantities. First, the dilatancy at the base ψ_b is related to the volume fraction by relation (3.20) the evolution of which is controlled by (3.18). Secondly, we have to express the basal shear rate $\dot{\gamma}_b$. As usual in the depth-averaged approach, we assume that, at each time, the velocity profile inside the layer has the same shape as the one predicted in the steady flows by the rheology. From (3.16) it is easy to show that the profile of a granular layer flowing down a slope is a parabola (Cassar *et al.* 2005). We then have the relation $\dot{\gamma}_b = 3\overline{u}^p/h$. This assumption means that the profile at each time is fully developed across the layer, which is not insured and will be discussed later in the paper. The remaining difficulty is to write the basal pressure p^p_b given by (3.13), in which the vertical velocity $\overline{v}^p$ comes into play. From dilatancy relation (3.18), we know that $\partial v^p/\partial z = \tan\psi\,\partial u^p/\partial z$. In the case of a dilatancy ψ independent of z, this equation can be integrated. However, in our avalanche, $\tan\psi$ *a priori* varies across the layer. It is then not possible to rigorously integrate this equation. We then assume in the following that the averaged vertical velocity is proportional to the averaged horizontal velocity times the basal dilatancy:

$$\overline{v}^p = K_4 \tan\psi_b \overline{u}^p, \tag{3.22}$$

where K_4 is a constant of order unity. This closure means that the dilatancy at the base gives the right order of magnitude of the dilatancy inside the layer. Finally, we assume that the thickness is constant $h \simeq h_0$ and that $\bar{\phi}h$, which is constant according to mass conservation (3.9), is equal to $\phi_c h_0$ where ϕ_c is the critical volume fraction introduced in (3.17). The final model describing the evolution of our avalanches is then given by the following set of equations, where we have dropped the averaged

bar symbol:

$$\rho_p \phi_c h_0 \frac{\mathrm{d}u^p}{\mathrm{d}t} = (\rho_p - \rho_f)\phi_c g h_0 \sin\theta - \tau_b^p + \frac{150\eta\phi^2}{(1-\phi)d^2}(u^f - u^p)h_0 \quad (3.23)$$

$$\rho_f (1-\phi_c) h_0 \frac{\mathrm{d}u^f}{\mathrm{d}t} = -\frac{150\eta\phi^2}{(1-\phi)d^2}(u^f - u^p)h_0 \quad (3.24)$$

$$\tau_b^p = (\mu_s + \tan\psi_b)p_b^p + K_1 \frac{3\eta u^p}{h_0} \quad (3.25)$$

$$p_b^p = (\rho_p - \rho_f)\phi_c g h_0 \cos\theta + K_4 \frac{150\eta\phi^2}{(1-\phi)^3 d^2} h_0 u^p \tan\psi_b \quad (3.26)$$

$$\tan\psi_b = K_3(\phi - \phi_{eq}) \quad (3.27)$$

$$\phi_{eq} = \phi_c - K_2 \frac{3\eta u^p}{p_b^p h_0} \quad (3.28)$$

$$\frac{\mathrm{d}\phi}{\mathrm{d}t} = -3\phi \tan\psi_b \frac{u^p}{h_0} \quad (3.29)$$

We can summarize the physical meaning of all the terms. Equation (3.23) is the solid momentum equation, where the acceleration is balanced by the gravity, the basal friction and the drag proportional to the relative motion between the grains and the fluid. Equation (3.24) stipulates that the fluid acceleration is driven by the drag only. Basal shear stress (3.25) is composed of three terms: a constant friction, a friction induced by the dilatancy and a viscous term. The normal granular pressure (3.26) is given by the relative weight of the grains plus a drag force induced by the dilatancy. Equation (3.27) says that the dilatancy is related to the difference between the volume fraction and the equilibrium volume fraction which is given by (3.28) and depends on the granular velocity and pressure. Finally, (3.29) gives the variation of the volume fraction as a function of the dilatancy.

It is standard practice in fluid mechanics to write dimensionless equations. In order to do so, we choose the initial thickness h_0 as a characteristic length scale, and a characteristic velocity scale U_0 given by

$$U_0 = \frac{(\rho_p - \rho_f) g h_0^2 \phi_c \cos\theta}{3K_1\eta}.$$

The time evolution of the fluid velocity, the grains velocity and the volume fraction are then given by the following equations where tilde means dimensionless quantities:

$$Fr^2 \frac{\mathrm{d}\tilde{u}^p}{\mathrm{d}\tilde{t}} = \tan\theta - \tilde{\tau}_b^p + \frac{\phi^2}{(1-\phi)} S(\tilde{u}^f - \tilde{u}^p) \quad (3.30)$$

$$\frac{\rho_f}{\rho_p} Fr^2 \frac{\mathrm{d}\tilde{u}^f}{\mathrm{d}\tilde{t}} = -\frac{\phi^2}{(1-\phi)} \frac{\phi_c}{(1-\phi_c)} S(\tilde{u}^f - \tilde{u}^p) \quad (3.31)$$

$$\frac{\mathrm{d}\phi}{\mathrm{d}\tilde{t}} = -3\phi\tilde{u}^p \tan\psi_b \quad (3.32)$$

$$\tilde{\tau}_b^p = (\mu_s + \tan\psi_b)\tilde{p}_b^p + \tilde{u}^p \quad (3.33)$$

$$\tilde{p}_b^p = 1 + \frac{\phi^2}{(1-\phi)^3} K_4 S \tilde{u}^p \tan\psi_b \quad (3.34)$$

$$\tan\psi_b = K_3(\phi - \phi_{eq}) \quad (3.35)$$

$$\phi_{eq} = \phi_c - \frac{K_2 \tilde{u}^p}{K_1 \tilde{p}_b^p} \quad (3.36)$$

where

$$Fr^2 = \frac{\rho_p U_0^2}{(\rho_p - \rho_f) g h_0 \cos\theta} \quad \text{and} \quad S = \frac{50}{K_1}\frac{h_0^2}{d^2}.$$

The initial conditions are $\phi = \phi_0$, and $u^f = u^p = 0$ at $t = 0$. In order to compare the prediction of this model with the experimental measurement we have simulated these equations using a fourth-order Runge–Kutta method.

3.5. *A typical simulation*

Before trying to quantitatively confront the model and the experiment, we first analyse qualitative features predicted by the theory.

First, it is interesting to note that the model predicts a flow threshold, which depends on the initial volume fraction. Equations (3.33) and (3.35) implies that no flow occur if the inclination is less than a critical angle θ_c verifying $\tan\theta_c = \mu_s + K_3(\phi_0 - \phi_c)$. The critical angle can then be higher or lower than the dynamics angle of friction if the initial volume fraction is higher or lower than the value ϕ_c.

A second remark concerns the short time evolution and the role of the inertial terms. In our configuration, a typical value of the Froude number is $Fr = 10^{-1}$. Under this condition, the dynamics is characterized by a very short initial phase on a dimensionless time scale of order Fr^2, followed by a much slower evolution. Using our experimental conditions, the typical time scale of this rapid phase is of order 10^{-2} s. Figure 4 shows typical evolutions of the different variables of the model in both a loose (dashed line) and a dense (solid line) cases. The short time evolution is plotted on the left of figure 4, and the long time on the right.

During the rapid initial transient, the particle phase accelerates (figure 4*a*) and the fluid velocity rapidly becomes equal to the particle velocity (inset figure 4*a*). During the same time, the pore pressure develops, and becomes negative in the dense case, and positive passing by an overshoot in the loose case (figure 4*c*). The dilatancy angle also varies during this initial accelerating phase especially in the loose case (figure 4*d*). The volume fraction is the only variable, which does not evolve on this rapid time scale (figure 4*b*). At the end of the transient inertial phase, the variables start to evolve on a much slower time scale.

The slow evolution is plotted in figure 4(*e–h*). First, one observes that both the dense and the loose cases converge towards the same steady state characterized by no dilatancy $\tan\psi = 0$, no pore pressure $\tilde{p}_b^f = 0$, by a terminal velocity $\tilde{u}_\infty^p = \tan\theta - \mu_s$ and a terminal volume fraction $\phi^\infty = \phi_c - K_2/K_1(\tan\theta - \mu_s)$. Secondly, the model predicts a dense and a loose behaviours similar to the ones observed experimentally. In the loose case, the velocity exhibits an overshoot due to the fact that the value reached during the initial rapid transient is higher than the value of the steady state (figure 4*e*). During the relaxation towards the steady state, the pore pressure is positive (figure 4*g*) and the dilatancy angle is negative (figure 4*h*), both relaxing to zero. The dense behaviour is characterized by an initial creep during which the velocity remains equal to its small value reached at the end of the rapid inertial phase. During this creeping time, the dilatancy angle decreases continuously to zero (figure 4*h*) and the pore pressure slightly decreases. When the dilatancy angle reaches zero, the avalanche starts: the velocity increases significantly and reach the steady-state value, while the pore pressure relaxes to zero.

The model exhibits a complex interplay between the dilatancy, the pore pressure and the acceleration and qualitatively mimics the major observations made in the experiments. The next step consists in estimating the different coefficients introduced

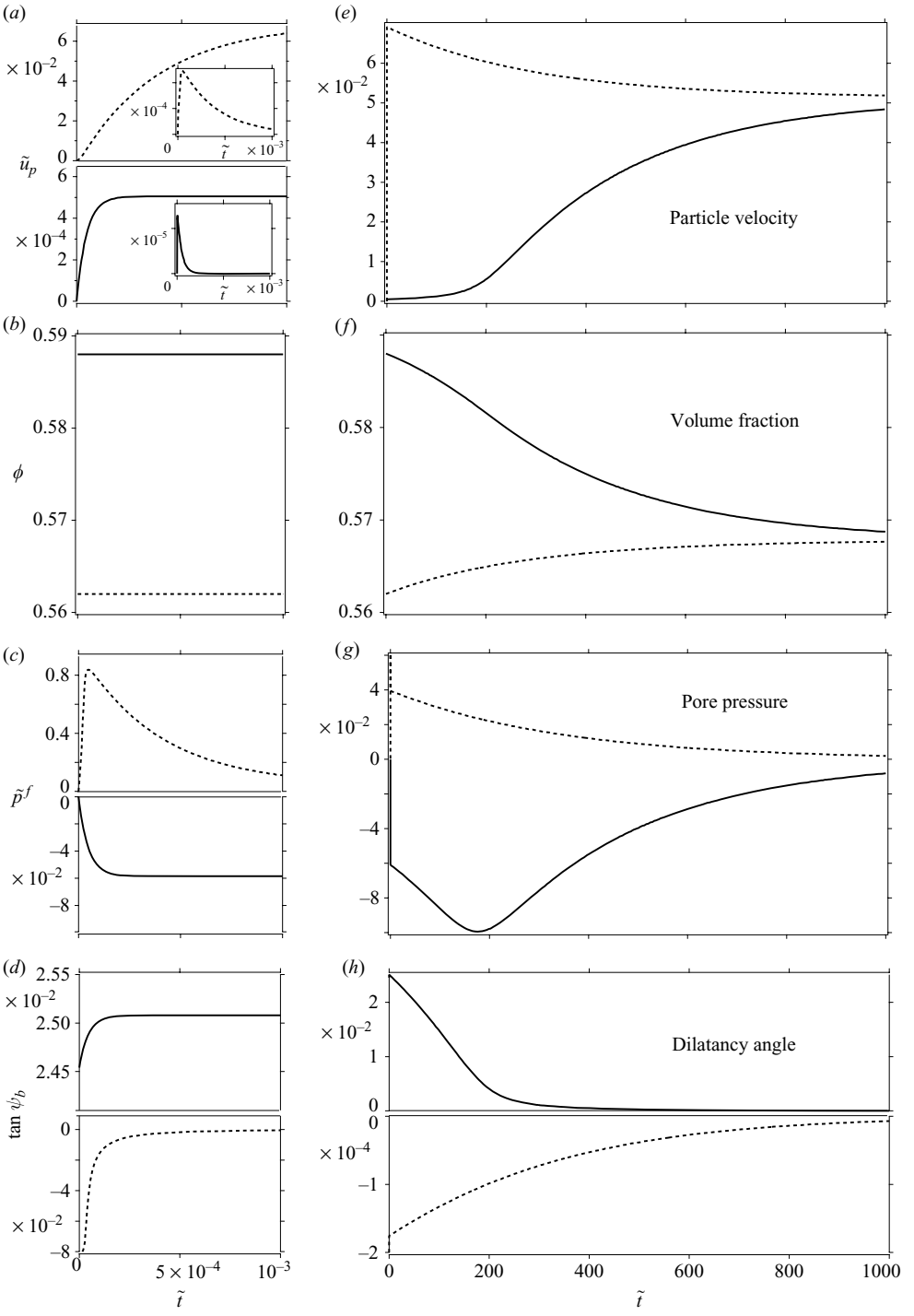

FIGURE 4. Typical simulations obtained for $S = 2403$, $\theta = 25^\circ$ for $\phi = 0.562$ (dotted line) and $\phi = 0.588$ (solid line); (*a–d*) short time evolution; (*e–h*) long time evolution; (inset) of (*a*) relative velocity $\tilde{u}_p - \tilde{u}_s$ between particles and liquid.

in the model to be able to quantitatively compare the experimental measurements with the theory. Before doing so, it is worth noting that the evolution of interest in the experiments corresponds to the slow evolution. A zero Froude number approximation can then be developed (appendix A), which is much faster to compute than the full original model. In this approximation the fluid velocity is equal to the solid velocity.

4. Quantitative comparison between experiments and theory

4.1. *Calibration*

Before comparing the theoretical predictions with the experiments, we need to determine the different parameters introduced in the model. The rheological parameters introduced are μ_s, K_1 in friction law (3.16) and ϕ_c and K_2 in dilatancy law (3.17). The calibration of the coefficients in our experiments is a difficult task, as the steady and fully developed regime is rarely achieved in our set-up. However, during the trials where a plateau in velocity was observed, we were able to obtain a good estimate of all the coefficients. Rheological model (3.23) and (3.25) predicts that the steady flow should verify $\tan\theta = \mu_s + K_1 I_b$ with $I_b = 3\eta u^p/(\Delta\rho g h^2 \phi_c \cos\theta)$. In figure 5(*b*) we have plotted the tangent of the inclination as a function of I_b, where I_b is computed using our measurement of the free surface velocity u_s^p in the steady regime and making the assumption that the profile is parabolic, i.e. $u^p = 2/3 u_s^p$. Although the collapse is not perfect, the data are compatible with the prediction, and the best linear fit gives $\mu_s = 0.415$ and $K_1 = 90.5$. Notice that the high value of K_1 justifies *a posteriori* the assumption that the viscous shear stress induced in the liquid phase is negligible (see appendix C).

The volume fraction parameters ϕ_c and K_2 are also difficult to be determined. The parameter ϕ_c is determined by discriminating between the dense and the loose behaviour from figures 2 and 3. We choose $\phi_c = 0.582$. To measure K_2 we use the following method. It can be shown in the model that for the dense situations when the avalanche starts, the volume fraction is close to its equilibrium value $\phi_{eq} = \phi_c - K_2 I_b$ (inset of figure 5*b*). If for each time during this phase, we plot the volume fraction ϕ measured experimentally as function of I_b measured at the same time, we obtained figure 5(*b*). One clearly observes that when the velocity increases, the volume fraction decreases. The different points correspond to different inclinations, different thicknesses and different viscosities. Despite the high dispersion, the data has a tendency to collapse along a line showing that the proposed scaling (3.17) $\phi = \phi_c - K_2 I_b$ is correct. The slope of the line passing by ϕ_c and parallel to the data gives $K_2 = 25$.

Another parameter in the model is K_3, which relates the dilatancy angle to the volume fraction (3.35). To determine K_3, we have studied how the critical angle below which no flow is observed varies when varying the initial volume fraction ϕ_0. We have seen that the model predicts that no flow is initiated if $\tan\theta < \mu_s + K_3(\phi_0 - \phi_c)$. Figure 5(*c*) shows the frontier between flow and no flow in the plane $(\phi_0, \tan\theta)$. The best linear fit gives $K_3 = 4.09$. The last parameter is K_4 introduced to relate the vertical velocity to the horizontal one (3.22) and which should be of order one. We have not found any simple way to measure this parameter and have fixed its value to 1.8, corresponding to the best fit we can get for the time evolution in figure 3.

All the parameters of the model being now determined, predictions for the whole avalanche dynamics can be compared with the observations.

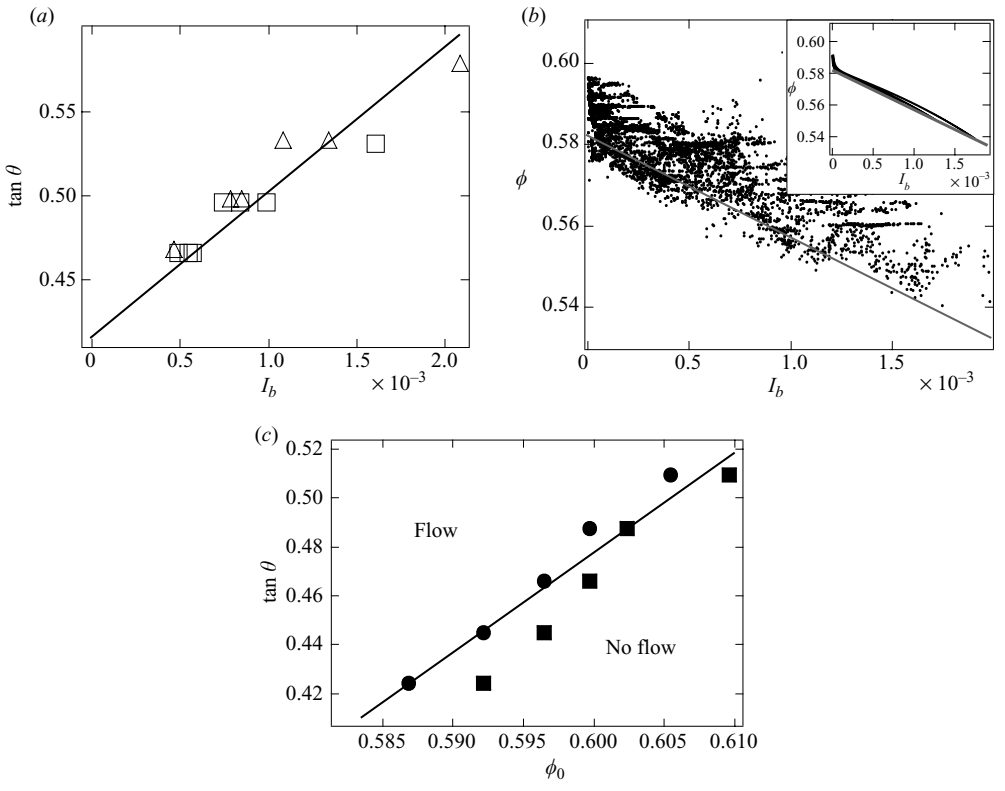

FIGURE 5. Calibration of the model: (*a*) friction law: $\tan\theta$ as a function of I_b (see text for definition) for steady states obtained with the low viscosity fluid (△) and with the high viscosity fluid (□). (*b*) Volume fraction: volume fraction as a function of I_b at different time of the dynamics, for different thicknesses (3.7 mm, 4.9 mm and 6.1 mm) and different angles (25°, 26.4°, 28° and 30°); (inset) theoretical evolution of $\phi(I_b)$ during the acceleration phase showing that it remains close to $\phi_{eq}(I_b)$ (straight line). (*c*) Flow threshold in the plane ($\tan\theta$,ϕ_0), a circle means that the granular layer prepared at the volume fraction ϕ_0 starts to flow when inclined at θ, a square means that the granular layer does not flow. The solid lines are the linear functions, which have been chosen to calibrate the model.

4.2. *Quantitative comparison*

In figures 2(*c, d*) and 3(*c, d*), the predictions of the model are plotted for both the high and the low viscosity cases. The agreement, although not perfect, is correct for both viscosities. The time evolution of the free surface velocity is quantitatively predicted for the different initial volume fractions, and the loose and the dense regimes are predicted in the theory for the same range of volume fraction. The characteristics of the dense cases are well captured by the model: the predicted creeping time is correct and the avalanche dynamics after the creeping regime is independent of the initial volume fraction as observed experimentally. The loose case behaviour is also captured by the model, with the existence of a velocity overshoot in the same range of volume fraction as observed experimentally. However, the initial acceleration of the granular layer when starting from a loose packing is overestimated by the model compared to the experiments. To compare more systematically the experiments and the theory, we have plotted for the dense cases the time delay t_{trig} necessary for the avalanche to start as a function of the volume fraction for different inclinations (figure 6).

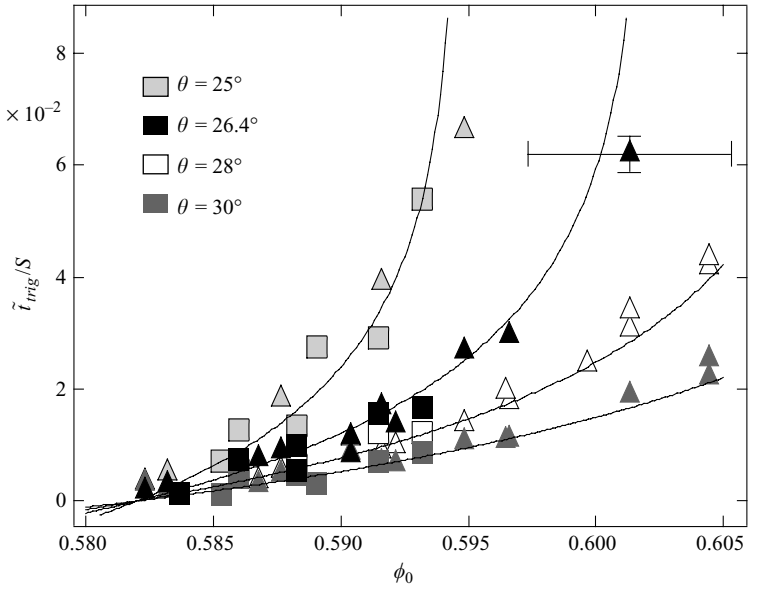

FIGURE 6. Dimensionless triggering time rescaled by the parameter S, $\tilde{t}_{trig}/S$ as a function of the initial volume fraction ϕ_0 for the low viscosity fluid (triangles), and for the high viscosity fluid (squares) at different inclinations. Solid lines are the theoretical predictions given by (B 4).

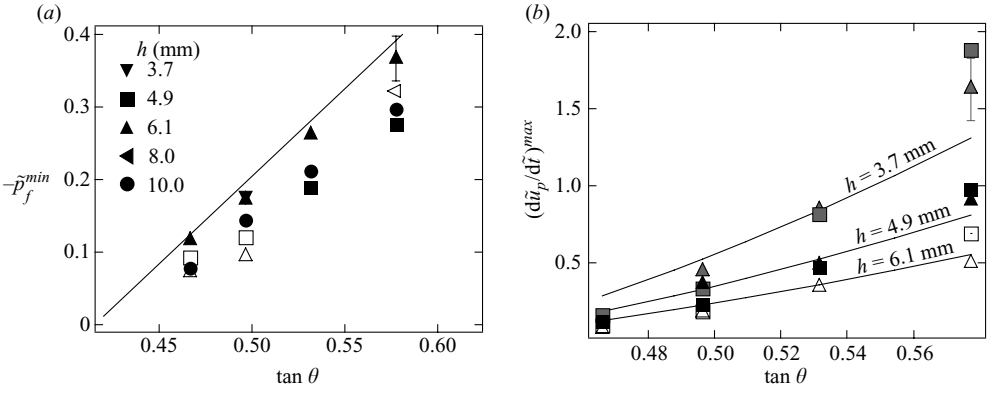

FIGURE 7. (*a*) Minimum of the dimensionless pore pressure measured in dense cases as a function of the inclination for different thicknesses; low viscosity (close symbols), high viscosity (open symbols). Solid line is the prediction of the model (*b*) dimensionless maximum acceleration for dense cases as a function of θ for different thicknesses, for the low viscosity fluid (triangles), and for the high viscosity fluid (squares). Solid lines are the predictions of the model.

The data are in a dimensionless form and the continuous lines are the theoretical predictions. It can be shown analytically (see appendix B) that $\tilde{t}_{trig}/S$ is a function of the inclination θ and of the initial volume fraction ϕ_0. The experimental data obtained for different viscosities, different inclinations, follow the predicted scaling. Another comparison between the experiments and the theory is given in figure 7(*b*). We have recorded for the dense cases the maximum acceleration reached during the avalanche. It does not depend on the initial volume fraction and only depends on the inclination

and on the thickness of the layer. Again, the data obtained for different viscosities follows the predicted scaling and are in agreement with the theoretical predictions within 20 %.

The final comparison concerns the pore pressure measurements. The theoretical predictions are plotted in figures 2(*d*) and 3(*d*). The time evolution of the pore pressure follows roughly the experimental measurements. A striking result obtained in our simulation is that the minimum pore pressure obtained in the dense case does not depend on the initial volume fraction (figure 2*d*). This is observed experimentally, and moreover, the measured minimum pore pressure is quantitatively in agreement with the theory (figure 7*a*). In conclusion, the theoretical model once calibrated quantitatively capture the rich dynamics observed during the initiation of the underwater avalanches.

5. Conclusion

To describe the initiation of underwater granular flows and the crucial role played by the initial volume fraction, a model has been developed based on a depth-averaged version of the two-phase flow equations. Special care has been taken in developing constitutive equations for the granular phase. By combining a critical state theory developed in soil mechanics and a rheological model issued from studies on steady granular flows, we have been able to propose a set of constitutive equations, which can take into account both the dilatant behaviour of the granular medium when it starts to deform and the steady flow regime. When the constitutive laws are introduced in the two-phase flow equations, the evolution of the underwater avalanche and the crucial role of the initial volume fraction are predicted. The different behaviours observed with loose and dense samples are captured by the model. For the dense cases, the agreement is not only qualitative but quantitative when the parameters of the model are calibrated using the steady flow regime. The relative good agreement between experiment and theory suggests that the approach could be relevant to describe more complex situations.

The avalanche configuration of interest in the present study is much simpler than the ones encountered in natural events. The flow is uniform, the grains are fully immersed and the flow is initiated by a sudden tilt of the granular layer. Several modifications are necessary to address the more complex problems posed by geophysical events such as landslides. First, the rheological behaviour of the granular phase has to be modified. The choice made in the present paper corresponds to a viscous regime suitable for our small-scale experiment. However, for real events, the rheology belongs to an inertial regime rather than a viscous one, as emphasized by Berzi & Jenkins (2008*a*, *b*). The dilatant–contractant constitutive laws developed in this paper can be easily adapted to the inertial regime by simply using (3.14) and (3.15) in constitutive laws (3.19) and (3.20). A second improvement of the model is to account for non-uniform flows and for variations in the water level. The derivation by Pitman & Le (2005) gives a relevant framework in which the constitutive relations developed in this paper can be implemented. The triggering of landslide induced by a slow increase of the water content as performed in the experiments by Iverson *et al.* (2000) could then be described.

The next extension of the model would be to go beyond the depth-averaged approximation. During the depth-averaging process we have made strong assumptions: the shape of the velocity profile is assumed to be parabolic and the dilatancy is assumed to occur everywhere in the layer. If these assumptions are

reasonable for thin layers, they will certainly fail in the case of thick layers. Variations across the layer are expected to occur. The present approach should then be extended by considering the full set of equations (3.5)–(3.8), a task postponed to future studies.

This work has benefited from fruitful discussions with Pascale Aussillous, Maxime Nicolas and Prabhu Nott. It has been supported by the Indo-French Centre for the Promotion of Advanced Research (IFCPAR) and by the Agence National de la recherche (ANR) through the PIGE Project.

Appendix A. Zero Froude number approximation

Neglecting the inertial terms in (3.30) and (3.31) implies that the fluid velocity is equal to the solid velocity. The momentum equation reduces to the following expressions:

$$\tan\theta = (\mu_s + \tan\psi_b)\tilde{p}_b^p + \tilde{u}^p, \tag{A 1}$$

$$\tilde{p}_b^p = 1 + K_4 S \frac{\phi^2}{(1-\phi)^3}\tilde{u}^p \tan\psi_b. \tag{A 2}$$

From those equations we obtain

$$\tilde{u}_p = \frac{\tan\theta - \mu_s - \tan\psi_b}{1 + K_4 S \frac{\phi^2}{(1-\phi)^3}\tan\psi_b(\mu_s + \tan\psi_b)}. \tag{A 3}$$

This last relation together with (3.35) and (3.36) allows to relate the dilatancy angle $\tan\psi_b$ to the volume fraction ϕ through a second-order equation.

$$\tan^2\psi_b\left[K_1K_4S\tfrac{\phi^2}{(1-\phi)^3}\tan\theta\right] + \tan\psi_b\left[K_1 + K_2K_3 - K_1K_3K_4S\tan\theta\tfrac{\phi^2}{(1-\phi)^3}(\phi-\phi_c)\right] - K_1K_3(\phi-\phi_c) - K_2K_3(\tan\theta-\mu_s) = 0. \tag{A 4}$$

Equations (A 3), (A 4) and (3.32) define the simplified system of equations to be solved in the zero Froude number approximation. The initial conditions are then only determined by the volume fraction ϕ_0, the initial velocity being non-zero and given by (A 3) and (A 4).

Appendix B. Estimate of the triggering time in the dense case

For the dense case, we can use (A 1) and (A 2), under the assumption, $\tilde{u}_p \ll 1$ during the creeping time. Equation (A 1) becomes

$$\tan\theta = (\mu_s + \tan\psi_b)\left(1 + K_4 S \frac{\phi^2}{(1-\phi)^3}\tilde{u}^p \tan\psi_b\right) \tag{B 1}$$

$$\tilde{u}^p \tan\psi_b = \frac{1}{SK_4}\frac{(1-\phi)^3}{\phi^2}\left[\frac{\tan\theta}{\mu_s + \tan\psi_b} - 1\right] \tag{B 2}$$

(3.32) and (3.35) lead to

$$-\frac{\dot{\tan\psi_b}(\mu_s + \tan\psi_b)}{\tan\theta - \mu_s - \tan\psi_b} = \frac{3K_3}{K_4 S}\frac{(1-\phi)^3}{\phi}. \tag{B 3}$$

Assuming $\phi = \phi_c$ in the left-hand side of (B 3), we integrate (B 3) with the boundary conditions $\tan\psi_b = \tan\psi_0 = K_3(\phi_0 - \phi_c)$ at $\tilde{t} = 0$ and $\tan\psi_b = 0$ at $\tilde{t} = \tilde{t}_{trig}$, we find

$$\tilde{t}_{trig} = \frac{K_4 S}{3K_3}\frac{\phi_c}{(1-\phi_c)^3}\left[-\tan\psi_0 + \tan\theta \ln\frac{-\tan\theta + \mu_s}{\tan\psi_0 - \tan\theta + \mu_s}\right]. \tag{B 4}$$

Appendix C. Estimate of the viscous stresses induced by the fluid motion

The fluid motion during the avalanche induces additional stresses, which have been neglected in the model. In this appendix, we estimate to which extent this assumption is valid.

The first viscous contribution is the shear stress of the fluid within the granular layer, which is of order $\eta\dot{\gamma}_b$, where $\dot{\gamma}_b$ is the shear rate at the base. Considering that the particle shear stress is given by (3.21), and that $K_1 = 90$, we conclude that the viscous shear stress of the liquid phase is negligible compared to the viscous shear stress of the granular phase.

The second contribution comes from the viscous stress that develops at the free surface between the granular layer and the clear fluid. The order of magnitude of this stress is $\eta u_p/\lambda$ where λ is the thickness of the boundary layer, which develops in the clear fluid due to the motion of the granular layer. Without carrying a complete computation of the boundary layer diffusion, one can estimate λ as being equal to $\sqrt{\eta/t\rho_f}$. To get an estimate of the role of this term in the dynamics, one can consider the dynamics of a granular layer without taking into account the dilatancy effect ($\psi_b = 0$) and assuming $u^f = u^p$. Equation of motion (3.30) in terms of dimensionless variables then reduces to

$$Fr^2\frac{\mathrm{d}\tilde{u}^p}{\mathrm{d}\tilde{t}} = \tan\theta - \mu_s + \tilde{u}^p + \frac{1}{3K_1}\sqrt{Re}\frac{\tilde{u}^p}{\sqrt{\tilde{t}}} \tag{C 1}$$

with $Re = \rho_f U_0 h_0/\eta$. One can show that the last term on the right-hand side is negligible during the whole dynamics. At short time $\tilde{u}^p$ is close to zero and the acceleration is dominated by the gravity term $\tan\theta - \mu_s$. When time goes on, the viscous term $\tilde{u}^p$ coming from the granular rheology rapidly dominates the interfacial stress.

REFERENCES

Ancey, C., Coussot, P. & Evesque, P. 1999 A theoretical framework for granular suspensions in a steady simple shear flow. *J. Rheol.* **43**, 1673–1699.

Armanini, A., Capart, H., Fraccarollo, L. & Larcher, M. 2005 Rheological stratification in experimental free-surface flows of granular-liquid mixtures. *J. Fluid Mech.* **532**, 269–319.

Berzi, D. & Jenkins, J. T. 2008*a* A theoretical analysis of free-surface flows of saturated granular liquid mixtures. *J. Fluid Mech.* **608**, 393–410.

Berzi, D. & Jenkins, J. T. 2008*b* Approximate analytical solutions in a model for highly concentrated granular-fluid flows. *Phys. Rev.* E **78**, 011304.

Brady, J. F. & Bossis, G. 1988 Stokesian dynamics. *Ann. Rev. Fluid Mech.* **20**, 111–157.

Cassar, C., Nicolas, M. & Pouliquen, O. 2005 Submarine granular flows down inclined plane. *Phys. Fuids* **17**, 103301.

Courrech du Pont, S., Gondret, P., Perrin, B. & Rabaud, M. 2003 Granular avalanches in fluids. *Phys. Rev. Lett.* **90**, 044301.

Da Cruz, F., Emam, S., Prochnow, M., Roux, J. N. & Chevoir, F. 2005. Rheophysics of dense granular materials: discrete simulation of plane shear flows. *Phys. Rev.* E **72**, 021309.

Doppler, D., Gondret, P., Loiseleux, T. Meyer, S. & Rabaud, M. 2007 Relaxation dynamics of water-immersed granular avalanches *J. Fluid Mech.* **577**, 161–181.

Forterre, Y. & Pouliquen, O. 2008 Flow of dense granular media. *Ann. Rev. Fluid Mech.* **40**, 1–24.

GDR MiDi 2004 On dense granular flows. *Eur. Phys. J.* E **14**, 341–365.

Géminard, J. C., Losert, W. & Gollub, J. P. 1999 Frictional mechanics of wet granular material. *Phys. Rev.* E **59**, 5881–5890.

Hampton, M. A., Lee, H. J. & Locat, J. 1996 Submarine landslides. *Rev. Geophys.* **34**, 33–59.

Huang, N., Ovarlez, G., Bertrand, F., Rodts, S., Coussot, P. & Bonn, D. 2005 Flow of wet granular materials. *Phys. Rev. Lett.* **94**, 028301

Iistad, T., Marr, J. G., Elverhoi, A. & Harbitz, C. B. 2004 Laboratory studies of subaqueous debris flows by measurements of pore fluid pressure and total stress. *Marine Geol.* **213**, 403–414.

Imran, J., Parker, G., Locat, J. & Lee, H. 2001 One-dimensional numerical model of muddy subaqueous and subaerial debris flows. *J. Hydr. Engng* **127**, 959–968.

Iverson, R. M. 1985 A constitutive equation for mass–movement behaviour. *J. Geol.* **93**, 143–160.

Iverson, R. M. 1997 The physics of debris flows. *Rev. Geophys.* **35**, 245–296.

Iverson, R. M. 2000 Landslide triggering by rain infiltration. *Water Resour. Res.* **36**, 1897–1910.

Iverson, R. M. 2005 Regulation of landslide motion by dilatancy and pore pressure feedback. *J. Geophys. Res.* **110**, F02015.

Iverson, R. M. & Denlinger, R. P. 2001*a* Flow of variably fluidized granular masses across three-dimensional terrain 1. Coulomb Mixture theory. *J. Geophys. Res.* **106**, 537–552.

Iverson, R. M. & Denlinger, R. P. 2001*b* Flow of variably fluidized granular masses across three-dimensional terrain 2. Numerical predictions and experimental tests. *J. Geophys. Res.* **106**, 553–566.

Iverson, R. M. & Lahusen, R. G. 1989 Dynamic pore pressure fluctuations in rapidly shearing granular materials. *Science* **246**, 796–798.

Iverson, R. M., Reid, M. E., Iverson, N. R., Lahusen, R. G., Logan, M., Mann, J. E., & Brien, D. L. 2000 Acute sensitivity of landslide rates to initial porosity. *Science* **290**, 513–516.

Jackson, R. 1997 Locally averaged equations of motion for a mixture of identical spherical particles and a Newtonian fluid. *Ch. Engng Sci.* **52**, 2457–2469.

Jackson, R. 2000 *The Dynamics of Fluidized Particles*. Cambridge University Press.

Jain, N., Ottino, J. M. & Lueptow, R. M. 2004 Effect of interstitial fluid on a granular flow layer. *J. Fluid Mech.* **508**, 23–44.

Jop, P., Forterre, Y. & Pouliquen, O. 2006 A constitutive law for dense granular flows. *Nature* **441**, 727–730.

Legros, F. 2002. The mobility of long-runout landslides. *Engng Geol.* **63**, 301–331.

Major, J. J. & Iverson, R. M. 1999 Debris-flow deposition: effects of pore-fluid pressure ad friction concentrated at flow margins. *Geol. Soc. Am. Bull.* **111**, 1424–1434.

Morris, J. F. & Boulay, F. 1999 Curvilinear flows of noncolloidal suspensions: the role of normal stresses. *J. Rheol.* **43**, 1213–1237.

Okura, Y., Kitahara, H., Ochiai, H. Sammori, T. & Kawanami, A. 2002 Landslide fluidization process by flume experiments. *Engng Geol.* **66**, 65–78.

Ouriemi, M., Aussillous, P. & Guazzelli, E. In press. Bed-load transport by shearing flows *J. Fluid Mech.*

Pailha, M., Nicolas, M. & Pouliquen, O. 2008 Initiation of underwater granular avalanches: influence of the initial volume fraction. *Phys. Fluids* **20**, 111701.

Pastor, M., Quecedo, M., González, E., Herreros, M. I., Fernández Merodo, J. A. & Mira, P. 2004 Simple approximation to bottom friction for bingham fluid depth integrated models. *J. Hydr. Engrg* **130**, 149–155.

Pitman, E. B. & Le, L. 2005 A two-fluid model for avalanches and debris flows. *Phil. Trans. R. Soc.* A **363**, 1573–1601.

Reynolds, O. 1886. Dilatancy. *Nature* **33**, 429–430.

Rice, J. R. 1975 On the stability of dilatant hardening for saturated rock masses. *J. Geophys. Res.* **80**, 1531–1536.

Roux, S. & Radjai, F. 1998 Texture-dependent rigid plastic behaviour.In *Proceedings: Physics of Dry Granular Media*, September 1997, Cargèse, France, pp. 305–311 (eds. H. J. Herrmann *et al.*). Kluwer.

Roux, S. & Radjai, F. 2001 Statistical approach to the mechanical behaviour of granular media. In *Mechanics for a New Millennium* (eds. H. Aref & J. W. Philips), pp. 181–196. Kluwer.

Rudnicki, J. W. 1984 Effects of dilatant hardening on the development of concentrated shear deformation in fissured rock masses. *J. Geophys. Res.* **89**, 9259–9270.

Schaeffer, D. G. & Iverson, R. 2008 Steady and intermittent slipping in a model of landslide motion regulated by pore-pressure feedback. *SIAM Appl. Math.* **69**, 768–786.

Schofield, A. & Wroth, P. 1968 *Critical Soil Mechanics.* McGraw-Hill.

Wood, D. M. 1990 *Soil Behaviour and Critical State Soil Mechanics.* Cambridge University Press.